



Applications and Applied Mathematics: An International Journal (AAM)

Volume 19 | Issue 2

Article 3

6-2024

(R2078) Analyzing the Effects of Fifth and Seventh Order Terms in a Generalized Henon-Heiles Potential

Nandana Madhukara
Canyon Crest Academy

Follow this and additional works at: <https://digitalcommons.pvamu.edu/aam>

 Part of the Numerical Analysis and Computation Commons

Recommended Citation

Madhukara, Nandana (2024). (R2078) Analyzing the Effects of Fifth and Seventh Order Terms in a Generalized Henon-Heiles Potential, Applications and Applied Mathematics: An International Journal (AAM), Vol. 19, Iss. 2, Article 3.

Available at: <https://digitalcommons.pvamu.edu/aam/vol19/iss2/3>

This Article is brought to you for free and open access by Digital Commons @PVAMU. It has been accepted for inclusion in Applications and Applied Mathematics: An International Journal (AAM) by an authorized editor of Digital Commons @PVAMU. For more information, please contact hvkoshy@pvamu.edu.



Analyzing the Effects of Fifth and Seventh Order Terms in a Generalized Hénon-Heiles Potential

¹**Nandana Madhukara**

Department of Mathematics and Physics
Canyon Crest Academy
5951 Village Center Loop Rd
San Diego, California

¹nandana.madhukara@gmail.com

Received: October 2, 2023; Accepted: August 16, 2024

Abstract

The Hénon-Heiles system is a 2-dimensional axisymmetric Hamiltonian system that was first formed to determine the third integral of motion in galactic dynamics. After its inception, it has become a paradigm in dynamical systems due to its apparent simplicity but extremely complicated dynamical behavior. In this paper, we perform a series expansion up to the seventh order of a general potential with axial and reflection symmetries. After some transformations, this becomes a generalized Hénon-Heiles (GHH) system where we separate the fifth and seventh-order terms. We qualitatively analyze this system for energies near the threshold between bounded and unbounded motion with Poincaré sections and quantitatively analyze with Lyapunov exponents. We find that particles far from the critical energy demonstrate less chaos. Additionally, the fifth-order term creates more regularity while the seventh-order term does the opposite.

Keywords: Hénon-Heiles Potential; Nonlinear dynamics; Astrophysics; Numerical Simulation

MSC 2020 No.: 70F15, 70K55, 65P10, 65P20

1. Introduction

One of the most famous and well-studied dynamical systems is the Hénon-Heiles system (Henon and Heiles (1964)). In 1964, astronomers Michel Hénon and Carl Heiles came up with the Hénon-Heiles (HH) Hamiltonian to study the existence of third integrals; however, the applications of this system have gone far past its original intentions. Because this system is analytically very simple but produces very interesting and complex trajectories, the Hénon-Heiles system has been studied in contexts ranging from geodesics in general relativity (Dolan and Shipley (2016)) to quantum entanglement using squeezed coherent states (Joseph and Sanjuán (2016)). More recently, this system has crossed over with neural networks (Thapar (2023), Robinson et al. (2022), Mattheakis et al. (2022)).

Lots of work has been done generalizing the system into a generalized Hénon-Heiles (GHH) system. Around 1980, Frank Verhulst (Verhulst (1979)) performed a series expansion up to the fourth order of a general potential with axial and reflection symmetry now known as the Verhulst Potential. This potential has been used to study various topics like the orbital structure in the center of a triaxial galaxy with an analytical core (de Zeeuw (1985)), the correlation between the Lyapunov exponents and the size of the chaotic areas in the surface of section (Chandler and Gibson (1989)), and the escape zones in a quartic potential (Barbanis (1990)). Recently, the potential has been expanded to fifth order (Dubeibe et al. (2018)) and seventh order (Dubeibe et al. (2020), Zotos et al. (2021)).

In this paper, we also study a seventh-order GHH system. We specifically consider the expansion from Zotos et al. (2021) that contains two parameters δ and α for the fifth and seventh order terms, respectively. This allows us to *separately* study how the higher order terms affect the dynamics of the system, which has not been done before. Another difference between this work and previous work about seventh-order expansions is that we use different tools from nonlinear dynamics to study the system. Rather than focusing on classifying orbits using the Smaller Alignment Index (SALI), we create and study the Poincaré surface of sections and Lyapunov exponents for our dynamical system. All these differences allow us to gain a whole new understanding of the dynamics of the Hénon-Heiles system, such as how δ and α affect the chaos of the system, which has not been studied before.

The main application of this paper is in the field of astrophysics. The Hénon-Heiles potential is an example of an axisymmetric potential, making it a great model for stars orbiting in a galaxy. However, the uniqueness of the Hénon-Heiles system is that it exhibits regular and chaotic motion. Understanding chaos in the context of astrophysics is crucial since lots of astrophysical systems display chaotic dynamics. One of the most famous examples is the three-body problem (Newton (1726)), but there are other examples like chaotic behavior in the solar system (Laskar (1990), Lecar et al. (2001)) and chaotic behavior exoplanetary systems (Deck et al. (2012)). Therefore, studying the Hénon-Heiles helps us understand more about the chaotic nature of the universe. By looking at an analytically simple system, such as the Hénon-Heiles system, this paper aims to provide intuition and tools that are essential for studying more complex real astrophysical systems that may be chaotic.

The paper is organized as follows. In Section 2, we will give some background on the type of systems we will be studying and the tools we will be using. This section will also include the definition of our GHH system. Next in Section 3, we will calculate the critical energy levels between bounded and unbounded motion. Then, we will look at Poincaré sections and Lyapunov exponents of systems for different values of δ , α , and the energy, and we end the paper with conclusions we draw from these results.

2. Background

2.1. Bounded and Unbounded Orbits

In this paper, we study energy levels near the threshold between bounded and unbounded motion. To define bounded, we first plot the potential energy as a function of x and y . For example, Figure 1 is the plot of the HH potential where the equation of this potential is

$$\frac{1}{2}(x^2 + y^2) + \lambda \left(x^2y - \frac{y^3}{3} \right) \text{ for } \lambda = 1.$$

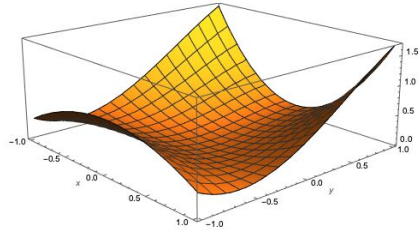


Figure 1. HH-system Potential Landscape

We call this surface a potential landscape. Now we can use this landscape to study the dynamics of objects under the influence of the potential. The main thing to note is that there can be valleys or local minimums in the surface where the object can get trapped. Now, we are ready to define what bounded motion is.

Let the object start at an energy E . As an example, Figure 2(a) would be the contour plot of the HH potential at $E = 1/8$. Notice the triangular loop in the center. If the object starts on that loop, it would get trapped there and would never escape, so we call the orbital motion bounded at $E = 1/8$. However, if E is greater than some critical value (in this case $E_{\text{crit}} = 1/6$), the contour plot would be like Figure 2(b) and have channels of escape.

2.2. Poincaré sections

One way we can analyze the Hénon-Heiles system is by using Poincaré surface of sections. The idea of Poincaré sections is to slice a higher dimensional phase space into a lower dimensional

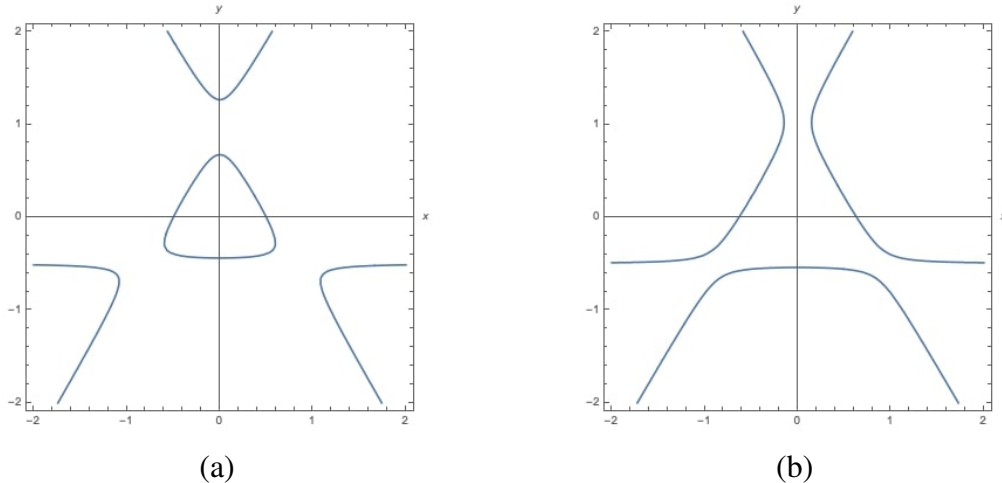


Figure 2. Contour plot at (a) $E = 1/8$ and (b) $E = 1/5$

space. Phase space is a space that represents all possible states of the system. So, the dynamics of a particle in a system can be thought of as movement in phase space. In our case, the phase space is 4-dimensional since its axes would be x, y, \dot{x}, \dot{y} . However, since energy is conserved, we effectively reduce down to a 3-dimensional phase space.

We can visualize this phase space with a 2-dimensional Poincaré section. We define our surface of section to be the \dot{y} vs y plane. For initial conditions, we set $x_0 = 0.1$, $y_0 = 0$, we pick a random value for \dot{y}_0 , and we find \dot{x}_0 by using conservation of energy: $\mathcal{H} = E$.

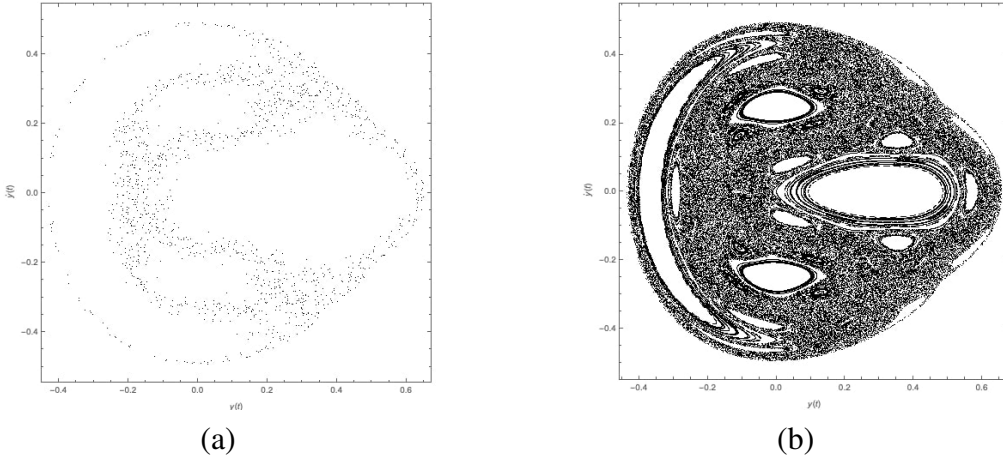
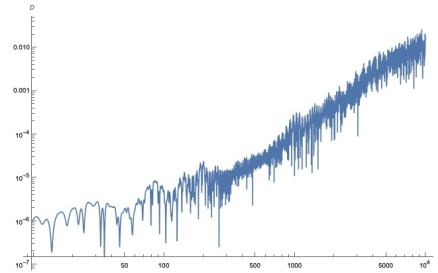
Now, the idea is that every time the trajectory goes through the surface of section, we draw a black dot at this point. If we do this for the Hénon-Heiles system for one initial condition and for a certain amount of time, we get Figure 3(a) which is when $E = 1/8$. Now we overlay the plot for different values of \dot{y}_0 so that we account for all allowed motion. This gives us Figure 3(b).

One of the main features of a Poincaré section is how it captures the chaos of the dynamical system. Therefore, the more random the surface of section looks, the more chaos the system exhibits.

2.3. Lyapunov Characteristic Exponents

Another tool we use to analyze the system, especially its chaos, are Lyapunov Characteristic Exponents (LCEs), which are a way of making chaos quantitative. Specifically in this project, we look at maximal LCEs. The main idea behind these exponents is to take two close trajectories and see how they grow apart or converge. If we take the Hénon-Heiles system, we can observe how two extremely close initial points grow apart. For our distance metric, we use the normal Euclidean distance between two points. When $E = 1/8$ and the initial separation is $D_0 = 10^{-6}$, we get the log-log plot of the distance shown in Figure 4.

If we let the distance be $D = D_0 e^{\lambda t}$, we can define λ to be our maximal LCE. Since we are using a

**Figure 3.** Poincaré sections of HH-system at $E = 1/8$ **Figure 4.** Contour Plot of HH Potential at $E = 1/8$

log-log plot, we can find λ by finding the slope of the line fit to this graph. In chaotic motion, two close initial points grow apart exponentially so a positive λ indicates chaotic motion. The larger λ is, the more chaotic the motion is.

For initial conditions, we set $x_0 = 0.1$, $y_0 = -0.1$, $\dot{y} = 0.0$, and solve for \dot{x} using conservation of energy: $\mathcal{H} = E$.

2.4. Generalized Hénon-Heiles Potential

In this paper, we use the same GHH Hamiltonian as the one in Zotos et al. (2021):

$$\begin{aligned} \mathcal{H} = & \frac{1}{2}(\dot{x}^2 + \dot{y}^2) + \frac{1}{2}(x^2 + y^2) + x^2y - \frac{y^3}{3} \\ & + \delta[x^4(y-1) + x^2(y-2)y^2 - y^4(y-1)] \\ & + \alpha[2x^6(y+1) + x^4y^2(2y+1) + x^2y^4(2y+1) + 2y^6(y+1)]. \end{aligned}$$

For this paper, we consider values of δ and α in the range $[0, 1]$.

3. Results

The first step we take is to find the boundary between bounded and unbounded motion (when we start near the origin). We get the following table of energies at the boundary:

$\alpha \setminus \delta$	0	0.1	0.5	1
0	0.1666	0.1046	0.0501	0.0323
0.1	0.2103	0.1168	0.0513	0.0326
0.5	0.2756	0.1843	0.0571	0.0339
1	0.3086	0.242	0.0693	0.0359

We call these energies E_{\min} and Figure 5 shows the contour plots when the energy is less than and greater than E_{\min} .

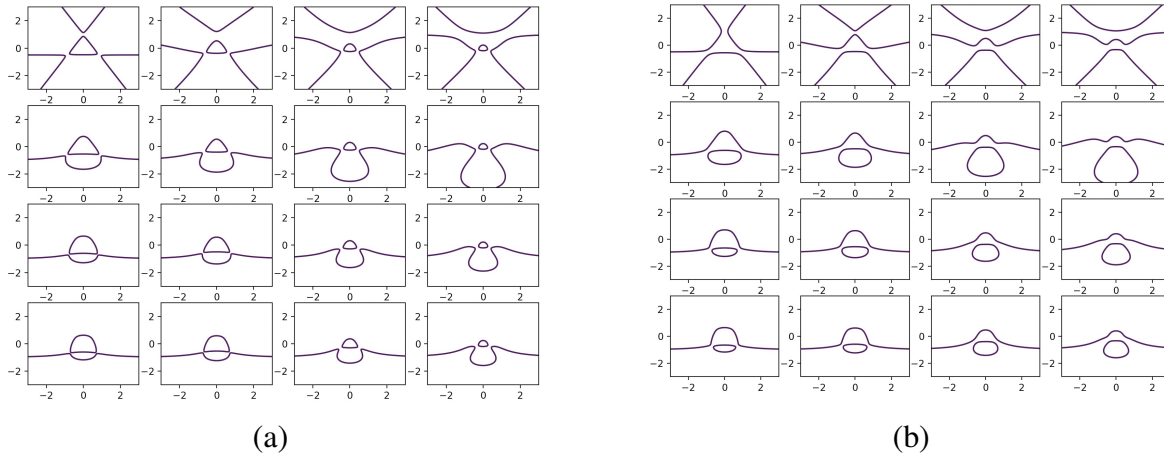


Figure 5. Transition from Bounded to Unbounded Motion

Next, we find the equations of motion by solving Hamilton's Equation:

$$\begin{aligned} \dot{x} &= p_x, \\ \dot{y} &= p_y, \\ \dot{p}_x &= -\frac{\partial \mathcal{H}}{\partial x}, \\ \dot{p}_y &= -\frac{\partial \mathcal{H}}{\partial y}, \end{aligned}$$

where p_x and p_y are the canonical conjugate momenta. After numerically solving these equations, we can start creating our Poincaré sections. For each value of α and δ , we will look at 3 different energy values so we will end up with 48 graphs. To make it simpler to look at, we split these into four 4×3 tables of graphs and we get Figures 8 to 11 (which can be found in the Appendices).

4. Analysis

First, notice that Figure 8(a) is the Poincaré section of the original HH-system. We can see that from the lack of structure and randomness in the plot, the system is chaotic which matches with the findings of Hénon and Heiles. From here, we can change 3 things: α , δ , and E . For now, let α be constant, so we first focus on Figure 8.

As we go from left to right, we see that more structure seems to emerge. For example, comparing Figure 8(a) to Figure 8(c), we can see that there are more loops rather than just noise. What this means is that as energy decreases and moves away from E_{\min} , the trajectories are less chaotic. Similarly, as we go down the table and δ increases, the chaos decreases. For α , we need to compare between different tables. We can use the (c) panel of all tables to see that in Figure 8, the Poincaré becomes more chaotic as we go from Figure 8 to Figure 11. Therefore, the chaos increases as α increases. We can now formulate all these observations into three points of the following theorem.

Theorem 4.1.

The GHH system follows the following properties:

- (1) As $E \rightarrow E_{\min}$, the chaos increases.
- (2) As $\delta \rightarrow 1.0$, the chaos decreases.
- (3) As $\alpha \rightarrow 1.0$, the chaos increases.

We can verify this theorem with the maximal LCE. We plot the maximal LCE λ against the energy, which we parameterize as $E = E_{\min}(1 - n/100)$, and we set $x_0 = 0.1$, $y_0 = -0.1$, and $\dot{y}_0 = 0.0$ as our initial conditions. See Figure 6.

In any of the plots, we can see that as $n \rightarrow 0$, which equivalent to $E \rightarrow E_{\min}$, the chaos $\lambda(n)$ increases, proving (1) in the Theorem. Additionally, we can see how λ depends on δ by looking at how λ changes at a specific value of n and α when we change δ , say at $n = 0$, $\alpha = 0$. See Figure 7(a).

We can see that as $\delta \rightarrow 1.0$, the height of the graph decreases and so does the Lyapunov exponent. This confirms (2) in the theorem. We can also see this trend in the Poincaré sections. For each 4 by 3 table of Poincaré sections, as we go down the table (which corresponds $\delta \rightarrow 1.0$), there is less noise and more structure. We can go through the same reasoning as $\alpha \rightarrow 1.0$, confirming (3) in the theorem. As we go through each table, the Poincaré sections develop more noise indicating that the chaos increases. The Lyapunov exponent also confirms this. See Figure 7(b).

5. Conclusion

In this paper, we have analyzed the dynamics of a seventh-order generalized Hénon Heiles system. We specifically, assigned separate parameters for the fifth and seventh-order terms to analyze each

of their effects. Then we looked at energies near the threshold between bounded and unbounded motion with three channels of escape. Through Poincaré sections and Lyapunov exponents, we were able to find how these different parameters affected the chaos demonstrated in the system. Specifically, we saw that energies close to the threshold between bounded and unbounded motion resulted in more chaos. We also found that increasing the effect of the fifth order decreases the chaos while the seventh order does the opposite.

Finally, it is worth noting that the Poincaré sections and Lyapunov exponents can be further used to gain a better understand of this system. For example, in addition to the amount of chaos in the system, Poincaré sections can also give information about the type of motion allowed in the dynamical system. For instance, some surface of sections like Figure 8(l) and 10(i) have lots of loops which indicates quasiperiodic motion. Further analysis can be performed on the shape of these loops to learn more about the fundamental frequencies of motion in this GHH system. Additionally, further numerical analysis can be done on the Lyapunov exponents to study the amount of effect δ and α have on the chaos. One of the intriguing parts of the result is that δ and α affect the chaos in different ways so this analysis could shine some light on why this difference exists.

REFERENCES

- Barbanis, B. (1990). Escape regions of a quartic potential, *Celestial Mechanics and Dynamical Astronomy*, Vol. 48, No. 1, pp. 57–77.
- Chandler, C. and Gibson, A.G. (1989). *N*-body quantum scattering theory in two Hilbert spaces. V. Computation strategy, *Journal of Mathematical Physics*, Vol. 30, No. 7, pp. 1533–1544.
- de Zeeuw, T. (1985). Motion in the core of a triaxial potential, *Monthly Notices of the Royal Astronomical Society*, Vol. 215, No. 4, pp. 731–760.
- Deck, K.M., et al. (2012). Rapid dynamical chaos in an exoplanetary system, *The Astrophysical Journal*, Vol. 755, No. 1. <https://doi.org/10.1088/2041-8205/755/1/121>
- Dolan, S.R. and Shipley, J.O. (2016). Stable photon orbits in stationary axisymmetric electrovacuum spacetimes, *Physical Review D*, Vol. 94, No. 4, pp. 731–760.
- Dubeibe, F.L., Riaño-Doncel, A., and Zotos, E.E. (2018). Dynamical analysis of bounded and unbounded orbits in a generalized Hénon–Heiles System, *Physics Letters A*, Vol. 382, No. 13, pp. 904—910.
- Dubeibe, F.L., Zotos, E.E., and Chen, W. (2020). On the dynamics of a seventh-order generalized Hénon–Heiles potential, *Results in Physics*, Vol. 18, pp. 103278.
- Henon, M. and Heiles, C. (1964). The applicability of the third integral of motion: Some numerical experiments, *The Astronomical Journal*, Vol. 69, No. 1, pp. 73–79.
- Joseph, S.K. and Sanjuán, M.A. (2016). Exploring chaos and entanglement in the Hénon–Heiles system using squeezed coherent states, *International Journal of Bifurcation and Chaos*, Vol. 26, No. 3, pp. 1650052.
- Laskar, J. (1990). The chaotic motion of the solar system: A numerical estimate of the size of the chaotic zones, *Icarus*, Vol. 88, No. 2, pp. 266–291. [https://doi.org/10.1016/0019-1010\(90\)90037-2](https://doi.org/10.1016/0019-1010(90)90037-2)

1035(90)90084-m

- Lecar, M., et al. (2001). Chaos in the solar system, *Annual Review of Astronomy and Astrophysics*, Vol. 39, No. 1, pp. 581–631. <https://doi.org/10.1146/annurev.astro.39.1.581>
- Mattheakis, M., Sondak, D., Dogra, A.S. and Protopapas, P. (2022). Hamiltonian neural networks for solving equations of motion, *Physical Review E*, Vol. 105, No. 6, pp. 065305.
- Newton, I. (1726). *Philosophiæ Naturalis Principia Mathematica*, Rare & Special e-Zone. <https://doi.org/10.14711/spc0/b706487>
- Robinson, H., Pawar, S., Rasheed, A. and Omer, S. (2022). Physics guided neural networks for modelling of non-linear dynamics, arXiv:2205.06858.
- Thapar, V. (2023). Applications of machine learning to modelling and analysing dynamical systems, arXiv:2308.03763.
- Verhulst, F. (1979). Discrete symmetric dynamical systems at the main resonances with application to axi-symmetric galaxies, *Philosophical Transactions of the Royal Society of London, Series A, Mathematical and Physical Sciences*, Vol. 290, No. 1375, pp. 435–465.
- Zotos, E.E., Dubeibe, F.L. and Riaño-Doncel, A. (2021). Fractal basins of convergence of a seventh-order generalized Hénon–Heiles potential, *Advances in Astronomy*, Vol. 2021, pp. 1-11.

APPENDIX

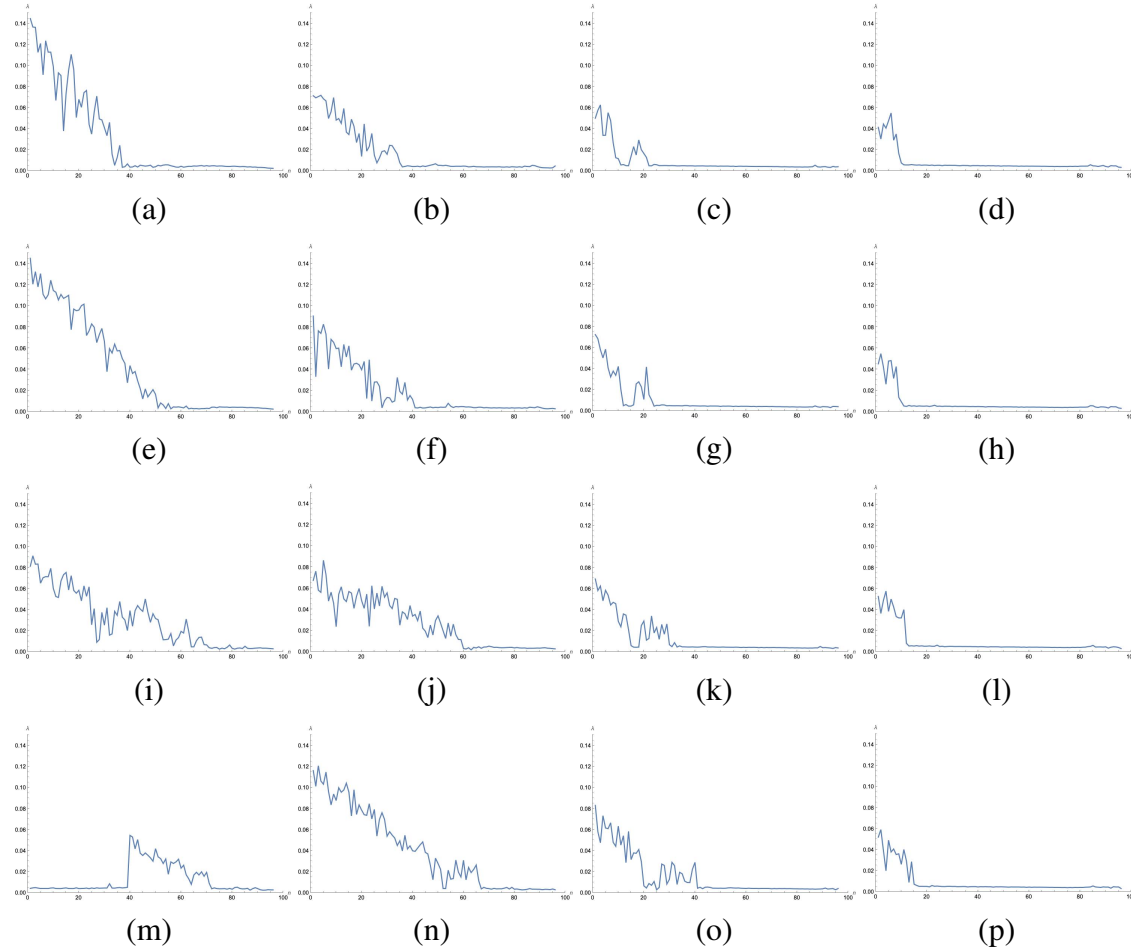


Figure 6. Maximal LCE vs Energy where α is 0, 0.1, 0.5, 1.0 from top to bottom and δ is 0, 0.1, 0.5, 1.0 from left to right

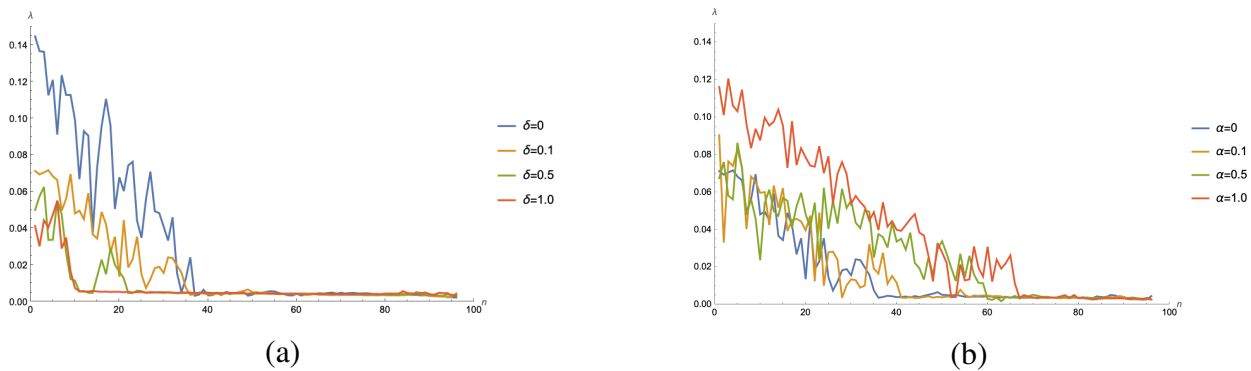


Figure 7. Maximal LCE vs Energy for (a) $\alpha = 0$ (b) $\delta = 0.1$

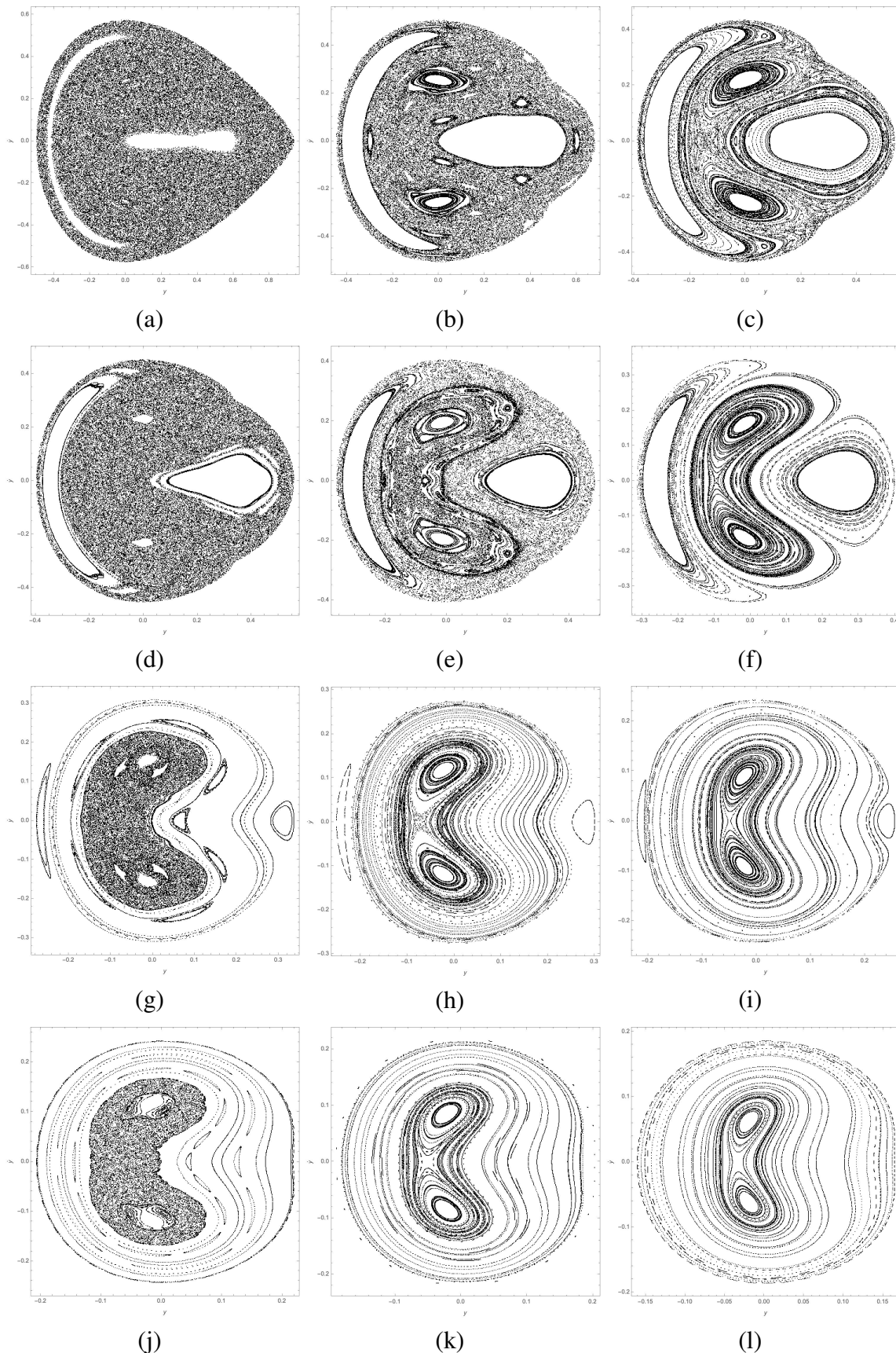


Figure 8. Poincaré sections when $\alpha = 0$ and (a) $\delta = 0$ and $n = 1$, (b) $\delta = 0$ and $n = 21$, (c) $\delta = 0$ and $n = 41$, (d) $\delta = 0.1$ and $n = 1$, (e) $\delta = 0.1$ and $n = 21$, (f) $\delta = 0.1$ and $n = 41$, (g) $\delta = 0.5$ and $n = 1$, (h) $\delta = 0.5$ and $n = 21$, (i) $\delta = 0.5$ and $n = 41$, (j) $\delta = 1.0$ and $n = 1$, (k) $\delta = 1.0$ and $n = 21$, (l) $\delta = 1.0$ and $n = 41$

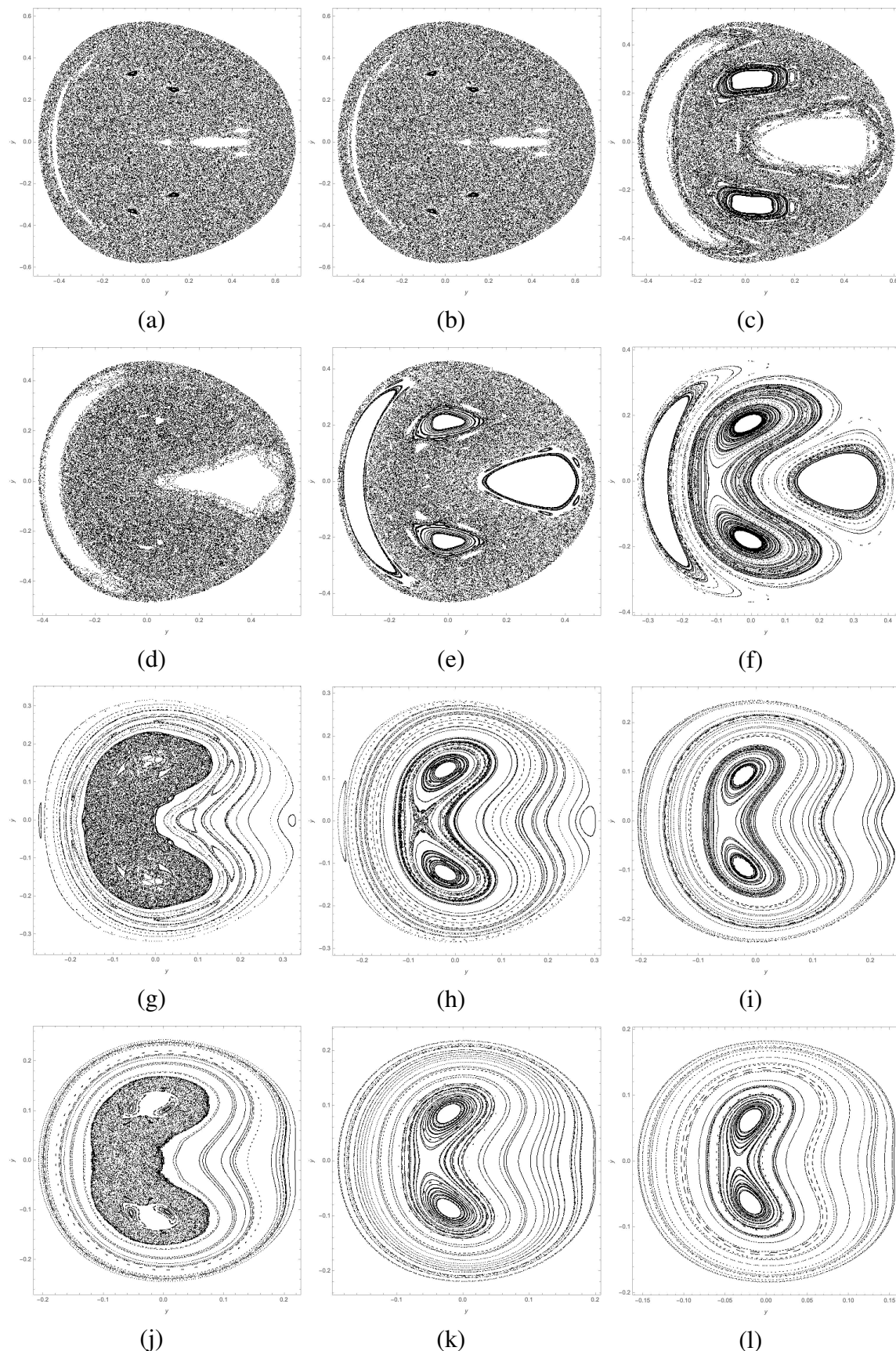


Figure 9. Poincaré sections when $\alpha = 0.1$ and (a) $\delta = 0$ and $n = 1$, (b) $\delta = 0$ and $n = 21$, (c) $\delta = 0$ and $n = 41$, (d) $\delta = 0.1$ and $n = 1$, (e) $\delta = 0.1$ and $n = 21$, (f) $\delta = 0.1$ and $n = 41$, (g) $\delta = 0.5$ and $n = 1$, (h) $\delta = 0.5$ and $n = 21$, (i) $\delta = 0.5$ and $n = 41$, (j) $\delta = 1.0$ and $n = 1$, (k) $\delta = 1.0$ and $n = 21$, (l) $\delta = 1.0$ and $n = 41$

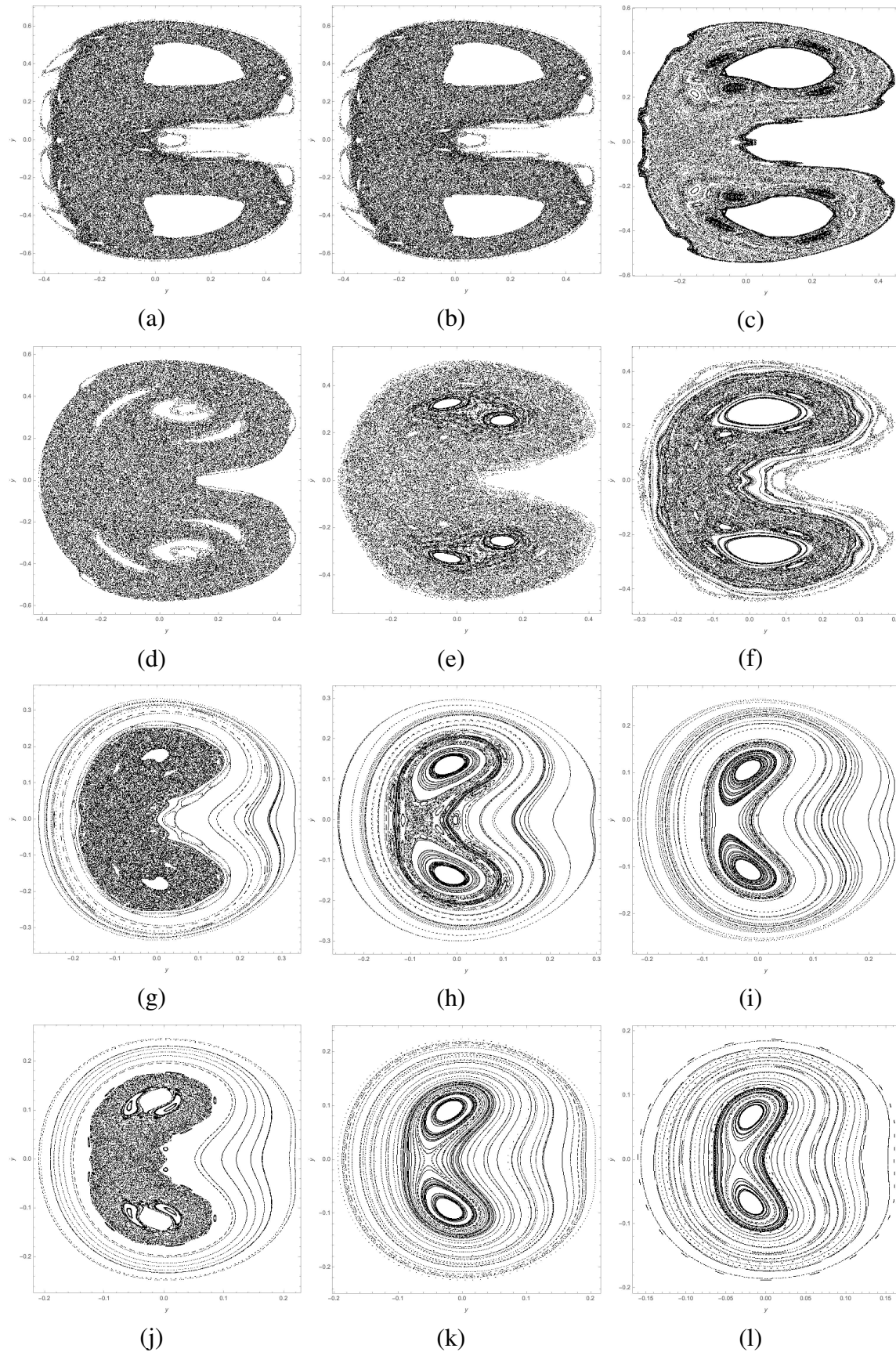


Figure 10. Poincaré sections when $\alpha = 0.5$ and (a) $\delta = 0$ and $n = 1$, (b) $\delta = 0$ and $n = 21$, (c) $\delta = 0$ and $n = 41$, (d) $\delta = 0.1$ and $n = 1$, (e) $\delta = 0.1$ and $n = 21$, (f) $\delta = 0.1$ and $n = 41$, (g) $\delta = 0.5$ and $n = 1$, (h) $\delta = 0.5$ and $n = 21$, (i) $\delta = 0.5$ and $n = 41$, (j) $\delta = 1.0$ and $n = 1$, (k) $\delta = 1.0$ and $n = 21$, (l) $\delta = 1.0$ and $n = 41$ where the energy for each panel is $E = E_{\min}(1 - n/100)$

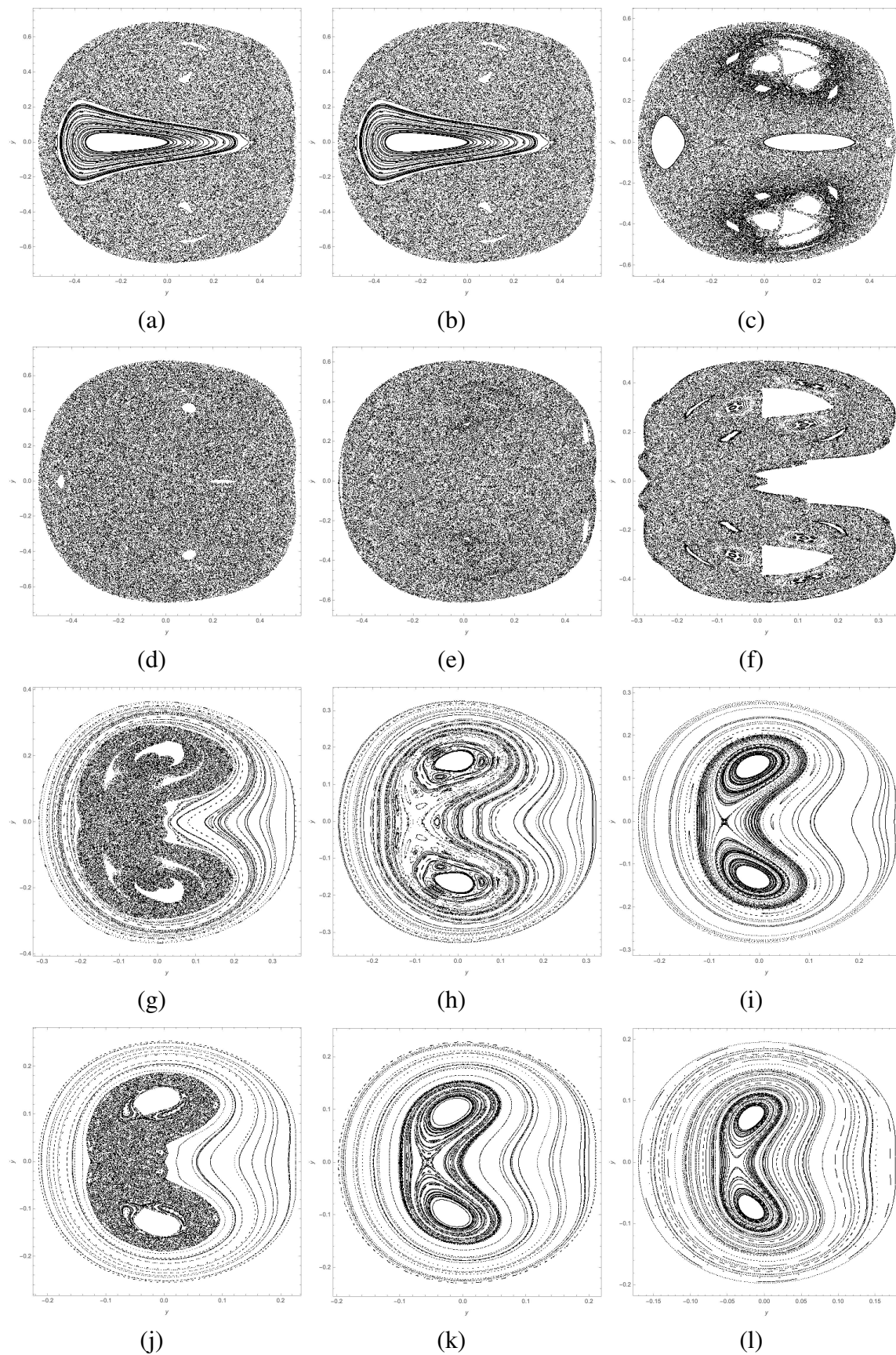


Figure 11. Poincaré sections when $\alpha = 1.0$ and (a) $\delta = 0$ and $n = 1$, (b) $\delta = 0$ and $n = 21$, (c) $\delta = 0$ and $n = 41$, (d) $\delta = 0.1$ and $n = 1$, (e) $\delta = 0.1$ and $n = 21$, (f) $\delta = 0.1$ and $n = 41$, (g) $\delta = 0.5$ and $n = 1$, (h) $\delta = 0.5$ and $n = 21$, (i) $\delta = 0.5$ and $n = 41$, (j) $\delta = 1.0$ and $n = 1$, (k) $\delta = 1.0$ and $n = 21$, (l) $\delta = 1.0$ and $n = 41$. The energy for each panel is $E = E_{\min}(1 - n/100)$